NeuroImage: Clinical 11 (2016) 423–434

Contents lists available at ScienceDirect

NeuroImage: Clinical

journal homepage: www.elsevier.com/locate/ynicl

Intraoperative optical mapping of epileptogenic cortices during non-ictal periods in pediatric patients

Yinchen Song[a], Jorge J. Riera[a], Sanjiv Bhatia[b], John Ragheb[b], Claudia Garcia[b], Alexander G. Weil[b], Prasanna Jayakar[b], Wei-Chiang Lin[a,*]

[a]Department of Biomedical Engineering, Florida International University, 10555 West Flagler Street, EC 2600, Miami, FL 33174, United States
[b]Division of Neurosurgery, Nicklaus Children's Hospital, 3100 SW 62nd Ave, Miami, FL 33155, United States

ARTICLE INFO

Article history:
Received 10 September 2015
Received in revised form 19 February 2016
Accepted 22 February 2016
Available online 26 February 2016

Keywords:
Intraoperative
Optical intrinsic signal imaging
Resting state
Epileptogenic
Eloquent

ABSTRACT

Complete removal of epileptogenic cortex while preserving eloquent areas is crucial in patients undergoing epilepsy surgery. In this manuscript, the feasibility was explored of developing a new methodology based on dynamic intrinsic optical signal imaging (DIOSI) to intraoperatively detect and differentiate epileptogenic from eloquent cortices in pediatric patients with focal epilepsy. From 11 pediatric patients undergoing epilepsy surgery, negatively-correlated hemodynamic low-frequency oscillations (LFOs, ~0.02–0.1 Hz) were observed from the exposed epileptogenic and eloquent cortical areas, as defined by electrocorticography (ECoG), using a DIOSI system. These LFOs were classified into multiple groups in accordance with their unique temporal profiles. Causal relationships within these groups were investigated using the Granger causality method, and 83% of the ECoG-defined epileptogenic cortical areas were found to have a directed influence on one or more cortical areas showing LFOs within the field of view of the imaging system. To understand the physiological origins of LFOs, blood vessel density was compared between epileptogenic and normal cortical areas and a statistically-significant difference ($p < 0.05$) was detected. The differences in blood-volume and blood-oxygenation dynamics between eloquent and epileptogenic cortices were also uncovered using a stochastic modeling approach. This, in turn, yielded a means by which to separate epileptogenic from eloquent cortex using hemodynamic LFOs. The proposed methodology detects epileptogenic cortices by exploiting the effective connectivity that exists within cortical regions displaying LFOs and the biophysical features contributed by the altered vessel networks within the epileptogenic cortex. It could be used in conjunction with existing technologies for epileptogenic/eloquent cortex localization and thereby facilitate clinical decision-making.

1. Introduction

Complete removal of epileptogenic brain areas in which seizures originate offers patients with refractory epilepsy the chance of being seizure free. However, this resection must be balanced against the preservation of eloquent cortical areas to reduce postoperative morbidity (Tharin and Golby, 2007). Many screening technologies based on the occurrence of both interictal and ictal abnormal activities have been used during the preoperative evaluation phase for epilepsy surgeries, including electroencephalograms (EEG), (functional) magnetic resonance imaging ((f)MRI), positron emission tomography (PET), and single-photon emission computed tomography (SPECT). Together, they provide the general location but not the exact boundaries of seizure-inducing brain areas. In addition, the usefulness of information provided by these non-invasive techniques degrades during the course of surgery because of brain shifting and deformation that is invariably induced by the loss of cerebrospinal fluid (Gasser et al., 2005; Winston, 2013).

Electrocorticography (ECoG) has been demonstrated to be a valuable intraoperative tool, not only to precisely delineate such boundaries (Alarcon et al., 1997), but also to identify eloquent cortical areas (Pondal-Sordo et al., 2007). However, the technique requires prolonged recordings with electrodes implanted long-term, thereby elevating the risks of hemorrhage, infection and cerebral edema. Intraoperative MRI (iMRI) and fMRI (ifMRI) have recently started to play crucial roles in epilepsy surgery, as they enable the maximum extent of resection despite the lesion's proximity to eloquent brain cortex and fiber tracts which, in turn, leads to favorable seizure-reduction outcomes and acceptable neurological deficit rates (Sommer et al., 2013). Unfortunately, the use of iMRI or ifMRI demands an extremely high standard of infrastructure and maintenance. As a result, only a limited number of hospitals and research institutes have the financial and technical capabilities to offer

* Corresponding author at: 10555 West Flagler Street, EC 2673, Miami, FL 33174, United States.
E-mail address: wclin@fiu.edu (W.-C. Lin).

http://dx.doi.org/10.1016/j.nicl.2016.02.015

these technologies for routine patient care. In addition, the functional mapping of ifMRI relies on the selection of hemodynamic response functions, which could compromise the accuracy of localization (Cannestra et al., 2001). Therefore, additional intraoperative evaluations are always needed to finalize the surgical plan and guide surgery.

Recently, dynamic intrinsic optical signal imaging (DIOSI) has been considered very useful as an alternative intraoperative technique to separate epileptic and tumorous cortices from eloquent brain areas (Haglund and Hochman, 2004; Sato et al., 2002; Sobottka et al., 2013). DIOSI is believed to hold great scientific potential that could both improve the interpretation of neuroimaging data and provide more detailed understanding about the cortical micro-environment. It has been suggested that DIOSI is capable of identifying epileptogenic cortex very well during ictal episodes, but it is impractical to implement such a localization technique in intraoperative settings, because seizure attacks are required. DIOSI can also be used for functional mapping, when external neuronal stimulation, like electrocortical stimulation (Cannestra et al., 2000; Suh et al., 2006) and/or peripheral stimulation (Sato et al., 2002; Sobottka et al., 2013) are applied. The dependence on external stimulation, however, requires delicate control of anesthetic administration to maintain the patient's consciousness, which could introduce additional risks to the surgery, especially in pediatric patients. Recently, Song et al. (2012) observed some unique hemodynamic low-frequency oscillations (LFOs, around 0.025 Hz) within very confined areas of the cortical surface of pediatric epilepsy patients undergoing epilepsy surgery. These areas were found to coincide with either epileptogenic or eloquent areas. However, methods to differentiate these two types of cortex using the observed LFOs were not explored. Therefore, improving the DIOSI technique's ability to delineate the epileptogenic cortices from the normal and eloquent areas using data recorded during non-ictal periods and without any stimulation would advance this modality as an intraoperative guidance tool.

In this study, a new methodology was developed to accurately delineate epileptogenic and eloquent cortices that requires only about 5 min of intraoperative DIOSI recording that occurs during spontaneous non-ictal periods. The proposed methodology focuses on functional and effective brain connectivity within cortical regions with LFOs, as well as on the anatomical and functional features of alterations in the vascular network of epileptogenic cortex. Its development is inspired by two past observations: 1) the existence of hemodynamic LFOs with possible neuronal sources in both epileptogenic and eloquent cortical areas during non-ictal periods (Song et al., 2012); and 2) seizure-induced reorganization of the vascular network in epileptogenic cortices (Rigau et al., 2007). There are three critical elements in this methodology. Specifically, a spontaneous DIOSI recording from the entire craniotomy is used to determine cortical regions with LFOs. To that end, we combine seed-based correlation, feature clustering and Granger causality analyses. Vessel densities in the superficial layers of the cortex are estimated using a static digital imaging modality for the entire craniotomy to uncover anatomical alterations in the vascular network of epileptogenic cortex. Finally, a stochastic modeling of vessel volume/oxygen dynamics based on the Balloon model (Buxton et al., 2004; Buxton, 2012) is combined with a machine learning method (i.e., a support vector machine, SVM) to differentiate areas with changes in vessel resistivity. Independent, routine ECoG analysis was performed by neurologists at Nicklaus Children's Hospital, and its results were used as the reference to confirm the localizations of epileptogenic and eloquent cortical areas and hence verify the accuracy of the proposed methodology.

2. Methods

2.1. Patient selection

This in vivo study was approved by the Western Institutional Review Board. Eleven patients (<18 years old) with lesional epilepsy undergoing one- or two-stage epilepsy surgery were chosen by their neurosurgeons (Dr. Bhatia and Dr. Ragheb) at Nicklaus Children's Hospital. Informed consent was obtained from each patient and their parents prior to surgery. Patients' demographic and clinical information are summarized in Table 1. The neurosurgeons were not aware of the results of this study at the time of surgery.

2.2. Optical data acquisition

Images at 500 nm and 700 nm were acquired simultaneously and continuously from the exposed cortical surface intraoperatively using a DOSIS system that had been developed in-house (Song et al., 2012). The exposed cortex was illuminated by the surgical light in the operating room and imaged through a Nikon dSLR lens (Nikon AF 28-80 mm f/3.5–5.6 D Lens with Aperture Ring). Images were re-collimated and then split into two branches using a dichroic mirror (#49–471, Edmund Optics) with a transmission wavelength range of 400–595 nm and a reflection wavelength range of 640–750 nm. Two CCD cameras (DMK 21 AU04, The Imaging Source Europe GmbH) were attached to the holder of the dichroic mirror: one at the transmission port (Cam_T) and the other at the reflection port (Cam_R). The Cam_T recorded images through a 500 nm band-pass filter (#65–149, Edmund Optics) and the Cam_R through a 700 nm band-pass filter (#88–012, Edmund Optics). Both cameras were synchronized using external triggers provided by a function generator. In each single-image acquisition sequence, at least 1000 frames were acquired by each camera at a rate of five frames per second. The imaging system was controlled by a LabVIEW program via an IEEE 1394a interface.

During each DIOSI study, the patient was kept still and his/her physiological condition kept stable under normal anesthesia. A list of anesthetic agents and other surgery-related information are provided in Table 2.

2.3. Electrocorticography (ECoG) acquisition and analysis

The procedures described in this section are part of the routine protocol provided to epilepsy surgery candidates at Nicklaus Children's Hospital. For patients undergoing two-stage epilepsy surgery, the ECoG electrode arrays were placed on top of the cortical surface following the optical imaging acquisition procedure. Placement of the ECoG electrode arrays was determined by the results of the pre-operative evaluations using scalp EEG, MRI/fMRI, PET and/or SPECT, which were not influenced by the results of DIOSI data analysis. After the first-stage surgery, the electrical activities of the target cortex of these patients were monitored for at least one week to identify the brain areas producing the ictal/interictal spikes. The final decision on the area of resection was determined by the ECoG results, in conjunction with those from the neuro-imaging studies. Once the surgery plan was finalized, these patients underwent the second stage of surgery to remove the electrode array and all epileptogenic brain areas. For patients undergoing one-stage epilepsy surgery, optical imaging acquisition was also performed prior to the confirmatory ECoG study, which was performed to identify the resection margin.

Neurologists at Nicklaus Children's Hospital analyzed all ECoG data and provided information on the localization of eloquent and epileptic cortical areas based on all neuro-imaging results (Jayakar et al., 1994, Jayakar et al., 2008). Eloquent areas are defined as cortical areas consistently related to a given function; e.g., sensory or motor. Epileptogenic cortex is considered an area of cortex that is required for seizure onset. Areas generating interictal spikes and discharges are also generally considered epileptic. DIOSI data analyses in the previous section were conducted without any knowledge of the results of the ECoG study. Later, the ECoG study results and the actual area of surgical resection were used as gold standards to define the epileptogenic and eloquent cortical areas.

Table 1
Individual demographic and clinical data on each of the eleven patients.

Patient	Gender	Age (y/o)	Stage	Craniotomy	Pathology	Follow-up duration (months)	Post-surgery outcome
1	Male	14	2	L F P	Tuberous sclerosis	18	No improvement. Still having seizures.
2	Female	17	2	R F T	FCD	12	No seizures
3	Female	7	2	R	Type 2 A FCD	31	Had auras. Now seizure free.
4	Male	12	2	L	n/a	9	No seizures
5	Male	16	2	R F T	Rasmussen encephalitis	32	Initially seizure free, now having seizures
6	Female	13	2	L F P T	Cavernous malformation	n/a	n/a
7	Female	15	2	L F T	Type 2A FCD; mild hippocampal gliosis	18	No disabling seizures. Seizure-free except for 2–3 seizures when anti-epileptic drugs stopped.
8	Male	8	2	L T	Cellular glial tumor; favor FCD	n/a	n/a
9	Male	9	2	R F T	Type 2A FCD	18	No seizures
10	Female	12	2	L T O	Gliosis	28	No seizures
11	Male	2 months	1	R F T	FCD	24	No seizures

y/o: years old; L: Left; R: Right; F: Frontal; T: Temporal; O: Occipital; P: Parietal; FCD: Focal cortical dysplasia; n/a: not available.

2.4. Optical data pre-processing

All optical data analyses were performed with MATLAB programs developed in-house following the steps shown in Fig 1A. Images from both cameras were co-registered and cropped to show the same exposed cortex area at two wavelengths and smoothed using a spatial averaging filter with a 3-by-3 square window. A time series for each pixel R(x,y,t) was analyzed, both in the time domain and the frequency domain. Since LFOs were of interest for this study, time series R(p,t), where p = (x,y), was filtered using a band-pass FIR filter (~0.02–0.1 Hz) which yielded $R_{low}(p,t)$. The FIR filter was designed in MATLAB using the Filter Design and Analysis Tool (fdatool) with an order less than a third of the data length. The artifacts in $R_{low}(p,t)$ originated from light source and vessel movements were removed using the principal component analysis (PCA) method, which produced $R_{PCA}(p,t)$. The power spectral density map (SDM, ~0.02–0.1 Hz) was generated using $R_{pca}(p,t)$ at each wavelength. A correlation coefficient map (CCM) was created by calculating the extent of correlation between $R_{pca}(p,t)$ at 500 nm and 700 nm for each pixel. Pixels displaying negative correlations were extracted from the CCM. Only those spatially-connected pixel groups were included in the following analyses. To remove those isolated pixels showing negative correlation, MATLAB function "bwconncomp" was used with an arbitrary threshold of 25 pixels to identify those spatially-connected pixel groups. These pixels were subsequently classified via the mean shift clustering method into multiple clusters based upon their temporal profiles in $R_{pca}(p,t)$ at both wavelengths. This classification was performed with no a priori knowledge about the number of existing clusters. $R_{pca}(p,t)$ in each cluster was then denoted as $R_{ci}(p,t)$, where subscript **i** stands for the cluster number.

2.5. Effective and functional connectivity

To understand effective connectivity in these clusters, a Granger causality toolbox (Luo et al., 2013) for non-stationary signals was applied to the mean values of $R_{ci}(p,t)$ at 500 nm ($\overline{R_{ci}}(p,t)$ in Fig. 1B). Influences that originated in a certain region and imposed on another were called "directed influences", since this effect flowed in a specific direction (Roebroeck et al., 2005). If $\overline{R_{ci}}(p,t)$ from region **A** was found to have a directed influence on the $\overline{R_{ci}}(p,t)$ of region **B**, region **A** would be denoted a Granger-cause (G-cause), while region **B** would be considered a Granger-effect (G-effect). When the directions of influence were identified, time series $\overline{R_{ci}}(p,t)$ at the G-causes and G-effects were used as a reference (i.e., seed) to calculate the seed-based correlation coefficients with $R_{pca}(p,t)$ from the other pixels within the field of view (FOV) at each wavelength, thereby demonstrating functional brain connectivity.

2.6. Alterations in vascular networks

Alterations in the vascular network of epileptogenic cortex were investigated through two different perspectives: anatomical and functional.

Table 2
Surgery-related data on the eleven patients.

Patient	Imaging time	Propofol, mg	Fentanyl, mg	Oxygen (L/min)	SEVO flurane (%)	Temperature	EKG	FIO_2 (%)	SpO_2 (%)	CO_2	PIP
1	10:30 am	100 (7:30 am)	25 (10 am)	2	2	36	SR	50	100	30	18
2	10:10 am	110 (8 am), 40 (9 am)	25 (9:45 am)	1.5	2	34.7	SR	50	100	27	15
3	9:10 am	n/a	10 (8:45 am)	2.5	2.5	34.6	SR	95	100	29	13
4	3:54 pm	100 (1:15 pm), 30 (2:30 pm)	50 (2:45 pm)	1	1.2	35.7	SR	40	100	32	12
5	9:22 am	130 (7:30 am)	50 (8:30 am, 9:30 am)	1	1.4	36	SR	40	100	33	17
6	12:32 pm	inf. 100 mg/kg per min	50 (12 pm)	1	0.5	37	SR	54	100	27	20
7	1:03 pm	150 (10 am), 100 (10:30 am)	50 (12:15 pm)	1	2.5	35.5	SR	40	100	36	18
8	11:04 am	inf. 100 mg/kg per min	100 (9:30 am)	2	n/a	35.7	SR	50	100	28	16
9	11:02 am	100 (8:15 am)	20 (9:45 am)	0.9	1.3	35	SR	35	100	27	16
10	10:29 am	inf. 50 mg/kg per min	50 (10 am)	1	0.7	35.7	SR	40	100	29	17
11	3:00 pm	n/a	5 (3 pm)	2	0.9	34.5	SR	50	100	32	16

SEVO flurane: sevoflurane;
EKG: Electrocardiogram;
FIO_2: Fraction of inspired oxygen;
SpO_2: Peripheral capillary oxygen saturation;
PIP: Peak inspiratory pressure;
inf: infusion;
SR: sinus rhythm;
n/a: not available.

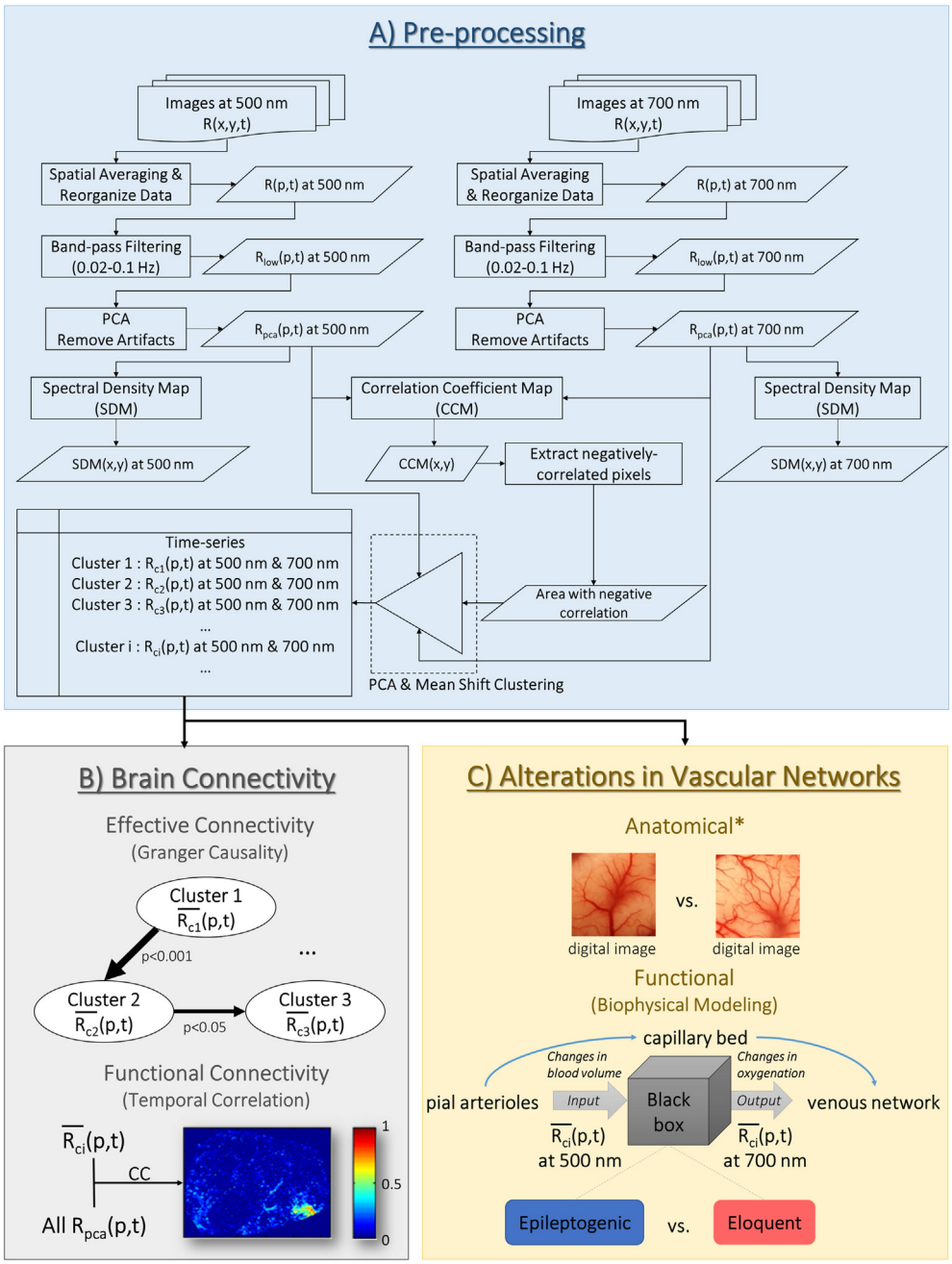

Fig. 1. Flow chart of the data analysis procedures used in proposed methodology. It consists of three major parts: A) pre-processing of optical imaging data, B) investigation based on brain connectivity (effective and functional connectivity), and C) quantitatively assessing the alterations in vascular networks from both anatomical and functional perspectives. The main goal of A) is to remove artifacts and extract negatively-correlated hemodynamic low-frequency oscillatory signals (LFOs). The LFOs were classified into multiple clusters based on their temporal profiles. The effective and functional connectivity of these clusters were investigated in B). To reveal the anatomical alterations in vascular network in C), digital images of the cortical surface were used to quantify the density of the superficial vascular network. The functional features of the altered vascular networks were assessed through a biophysical modeling approach to focus on the relationship between the local blood volume and oxygenation. PCA: principal component analysis. *Analyses on anatomical features of the vascular networks were performed based on digital images of the exposed cortical surface.

2.6.1. Anatomical features

To document the blood vessel network on the cortical surface with high spatial resolution, digital color images of the exposed cortex were acquired using a commercial-grade digital SLR camera (Sony α100) during surgery from Patients 1, 2, 5, 7, 8, and 9. The program ImageJ (http://imagej.nih.gov/ij/) was used to perform edge detections on these images and thereby identify the vessel network. Several image areas with the same dimensions (AOIs) were selected from the epileptogenic and normal cortex, as defined by the ECoG study results, within the same brain lobe for each patient. A histogram was generated from each AOI using its 8-bit post-processed image (the edges of the blood vessels highlighted), which indirectly quantified vessel density. Finally, the histograms of the AOIs from epileptogenic cortex ($n = 18$) were statistically compared against those from normal cortex ($n = 20$) using a non-parametric permutation test (10,000 times, $p < 0.05$). The null hypothesis of this permutation test was that the values in the histograms of two sets of AOIs at each intensity level (i.e., 0–255; for a total of 256 intensity levels) would follow the same distribution. Therefore, if the null hypothesis is true, the values in the histograms of AOIs are exchangeable between the two sets (i.e., epileptogenic and normal cortical

areas). For the permutation test, the histograms from epileptogenic and normal cortical areas were combined and randomly grouped into two different subsets 10,000 times. Each time, a two-sample, two-tailed t-test was performed on both subsets of data for each intensity level. Eventually, at each intensity level, 10,000 t-statistics were constructed from the random partitions. These 10,000 t-statistics were later compared with the observed t-statistics obtained without the random partitions. The proportion of random partitions that resulted in a larger t-statistic than that which was observed was the p-value (p) of this permutation test. If p was found to be less than the significance level (0.05), it meant that the blood vessel densities of the epileptogenic and normal cortical areas were significantly different.

2.6.2. Functional features–biophysical modeling

Based on the optical absorption spectra of oxy- and deoxy-hemoglobin, DIOSI data at 500 nm primarily reflect changes in cerebral blood volume (CBV). DIOSI data at 700 nm, on the other hand, are highly sensitive to hemoglobin oxygenation, because of the significant difference in the absorption coefficients between oxy- and deoxy-hemoglobin at this wavelength. Since both parameters are known to be affected by neuronal activity according to the Balloon model (Buxton, 2012), investigating the relationship between the DIOSI data at 500 nm and 700 nm would provide insights into the interplay between changes in CBV and oxygenation under the influence of both neuronal activity and metabolism. This, in turn, could offer a window of opportunity to separate epileptogenic from eloquent cortex using parameters that characterize the interplay between changes in CBV and oxygenation (Fig. 1C). To verify this hypothesis, $\overline{R_{ci}}(p,t)$ at both wavelengths with negative correlations from epileptogenic and eloquent cortical areas, as defined by the outcomes of the ECoG studies, were applied to an autoregressive model with an exogenous source (ARX) expressed as:

$$y_t = \phi_0 + \sum_{i=1}^{p} \phi_i y_{t-i} + \sum_{i=1}^{r} \psi_i u_{t-i} + \varepsilon_t, \quad (1)$$

where $\mathbf{u}$ is $\overline{R_{ci}}(p,t)$ at 500 nm (related to CBV) as the exogenous source (input of the system), $\boldsymbol{y}$ is $\overline{R_{ci}}(p,t)$ at 700 nm (reflecting variations in oxygenation) as the output of this stochastic system, $\boldsymbol{\Phi}$ and $\boldsymbol{\psi}$ are the coefficients for variables $\underline{\boldsymbol{y}}$ and $\boldsymbol{u}$, respectively, $\boldsymbol{p}$ and $\mathbf{r}$ are the order of the series for $\boldsymbol{y}$ and $\underline{\boldsymbol{u}}$, respectively, and $\boldsymbol{\varepsilon}$ is white noise. Theoretically, by calculating $\boldsymbol{\Phi}$ and $\boldsymbol{\psi}$, changes in oxygenation could be predicted from this ARX model, if the changes in CBV were known. Although this data-driven model does not strictly follow any biophysics-based mechanism, the impulse response functions (IRFs) of the model, to a certain extent, could indirectly indicate the relationship between changes in CBV and oxygenation, and hence contain useful features to differentiate eloquent from epileptogenic cortex. The concept behind the IRFs of this ARX model is similar to the hemodynamic response function used in event-related fMRI analysis (Glover, 1999).

2.6.3. Support vector machine

A support vector machine (SVM), a common machine-learning method that is frequently used in predictive modeling for clinical decision-making, was employed with quadratic programming to train the computer to identify the differences between the IRFs obtained from epileptogenic and eloquent cortical areas. SVM has primarily been employed in EEG analysis for seizure detection (Guo et al., 2010, Subasi and Gursoy, 2010 and Zavar et al., 2011). However, it has also been used as a diagnostic tool in anatomical and functional imaging studies (Chaplot et al., 2006, El-Naqa et al., 2002 and Ramírez et al., 2013). Here, $\overline{R_{ci}}(p,t)$ obtained from the epileptogenic and eloquent cortical areas were split into two parts: one was used as the training data set and the other as a testing data set. Each part was about 100 s long. Upon obtaining the estimated IRFs from each data set, Haar wavelet decomposition (Mallat, 1989) was employed to extract unique features from IRFs. The coefficients obtained from the Haar wavelet decomposition were scaled (i.e., standard deviation = 1) and centered (i.e., mean = 0). Coefficients would be used in the SVM as the features for training and testing purposes, if they were found to be significantly different between two groups of data using the non-parametric permutation test (refer to Section 2.6.1). Finally, the performance of the SVM with different orders of ARX model (p and r: 5–40) was empirically assessed in terms of its accuracy, sensitivity, specificity, and area under the receiver operating characteristic (ROC) curve.

3. Results

Eleven patients undergoing epilepsy surgery were enrolled in this study, and their individual demographic and clinical information, such as post-surgery outcome, are provided in Table 1. It should be noted that post-surgery outcomes were not affected by any of the DIOSI studies presented in this manuscript. Some patients (Patients 1, 5, and 7) were not completely seizure free after surgery, which could be due to incomplete resections of the lesion and electrographically-abnormal region (Paolicchi et al., 2000, Krsek et al., 2013) or insufficient pre-operative mapping of multi-focal lesions and/or epileptogenesis (Krsek et al., 2013). However, we elected to retain the results from these three patients in our analysis, since the ECoG analyses performed on these patients did succeed at locating the seizure-onset zones within the operative sites. The DIOSI study was performed twice in three of these patients (Patients 2, 4 and 7); each of these two studies possessed a unique view angle to the exposed cortex. Therefore, the analysis results from a total of fourteen image sequence sets are presented.

Fig. 2 is a sample image acquired with the DIOSI system (Fig. 2A, at 700 nm) versus a second image captured using a commercial-grade digital camera (Fig. 2B). Following DIOSI image acquisition, another picture of the exposed cortical surface was taken with the ECoG electrode array placed on top (Fig. 2C). Neurologists at Nicklaus Children's Hospital documented the locations of epileptic and eloquent cortical areas using the ECoG electrode number. In Fig. 2, the resection area, which is responsible for seizure onset, was outlined in light blue curve. With these three images, the results derived from DIOSI data analyses could be easily compared with those of ECoG data analyses.

3.1. Effective and functional connectivity

Consistent with the findings of Song et al. (2012), strong LFOs (<<0.1 Hz) were observed in all fourteen acquired data sets. A set of representative LFO analysis results from the same patient as Fig. 2 is presented in Fig. 3. In this case, negative correlations between intrinsic optical signals at both wavelengths were located in certain focal areas (Fig. 3E). Using k-means segmentation, negative-correlation areas greater than 100 pixels were separated from the remaining cortical areas (Fig. 3G). These areas included both epileptic cortex and normal eloquent areas. Intrinsic optical signals from these isolated areas were separated further into multiple clusters by simultaneously using the temporal features identified from both wavelengths (Fig. 3H). The 3-D scatter plot of the classified features is shown in Fig. 3I. Each cluster possessed a unique oscillation pattern (Fig. 3J), for which the spatial distribution could be scattered (Fig. 3H). As an example of the robustness of the classification process, Clusters 1, 2 and 3 in Fig. 3H are connected spatially, but the temporal profiles of their intrinsic optical signals at both wavelengths (Fig. 3J) are clearly different (marked in gray boxes). The same conclusion could be drawn from Clusters 4 and 5, as well.

To understand effective connections between these epileptic and eloquent areas, the directed influences between them were identified using the Granger causality method. In general, the clusters located

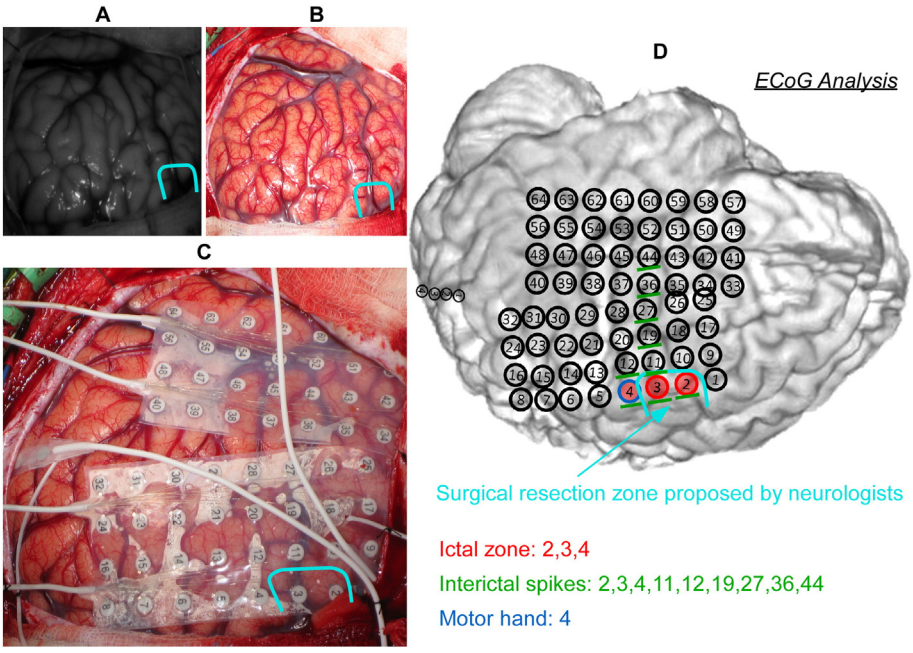

Fig. 2. An example of images acquired using the dynamic intrinsic optical signal imaging (DIOSI) system (A) and a commercial dSLR camera (B). An image also was captured with a dSLR camera after placement of the electrocorticography (ECoG) electrode array (C) for the purpose of a post-analysis comparison between DIOSI and ECoG analyses. (D) is an example of the result that the neurologists at Nicklaus Children's Hospital provided us with. The resection area for this patient (Patient 1) is outlined in light blue. Eloquent area was defined by direct cortical mapping with electrical current stimulation (Jayakar et al., 2008). (For interpretation of the references to color in this figure legend, the reader is referred to the web version of this article.)

inside the resection area, presumed to be related to seizure onset, were found to exert influences on other brain areas (Fig. 3K). However, not all the identified clusters exhibited causal relationships (e.g., Clusters 1, 2, and 4 in Fig. 3H), which might indicate that these areas were not effectively connected, regardless of their structural or functional connections. Once all the G-causes and G-effects were determined, the averaged intrinsic optical signals $\overline{R_{ci}}(p,t)$ within a G-cause area and a G-effect area were used as the seeds to obtain CCM based on seed-based correlations with intrinsic optical signals of all the other pixels $R_{pca}(p,t)$ at the corresponding wavelengths. It is clear that the correlated areas revealed at 500 nm (Fig. 3L and O) were much more focal than those at 700 nm (Fig. 3M and P), which could result from the longer optical path length for biological tissue at 700 nm.

Fig. 4 shows representative results from another studied patient (Patient 2) as a further example, and leads to similar conclusions with regards to the importance of LFO clustering, as well as the need to investigate effective connectivity. Unlike Patient 1 in Fig. 3, the G-cause (Fig. 4F) and G-effect (Fig. 4I) of Patient 2 seem to be temporally correlated (Fig. 4G, H, J and K). However, the Granger causality test indicated a difference between these two areas. Once again, the G-cause area is located inside the resection zone (outlined in yellow, Fig. 4F) and is responsible for seizure onset in Patient 2.

Among all fourteen imaging data sets, there were two cases (Patients 6 and 10) in which only eloquent areas were identified within the optical field of view (FOV). For these two cases, the resection areas were either below the cortical surface or adjacent to the craniotomy but covered by skull. Nevertheless, strong hemodynamic LFOs were found within the resection areas (i.e., epileptogenic areas) in all the remaining twelve cases. Seventy-five percent (9 out of 12) of the resection areas exhibited negative correlations between their intrinsic optical signals at 500 nm and 700 nm, and they had directed influences on other cortical areas. Meanwhile, 83% (10 out of 12) of the G-causes identified via the Granger causality method were related to epileptic activity (i.e., either ictal or interictal discharges), as shown in Fig. 5. However, eloquent areas could be the G-cause as well; on some occasions they either directly contributed to the activities in a distant cortex (both data sets of Patient 7) or relayed the activities from the epileptic cortex to some distant cortex (Patients 3 and 5, and both data sets of Patient 4). This indicates that eloquent cortical areas, if involved, may facilitate the propagation of epileptic activities through their network to remote cortical areas.

3.2. Vasculature abnormalities in the superficial layer–anatomical features

Because of the image quality and location of the resection zone, the high-resolution cortical surface images from just six patients were used for vasculature network characteristic analysis. Representative processed images, which show the edges of blood vessels, are shown in Fig. 6A. From the six processed images used, 18 sub-images and their histograms were obtained from epileptogenic cortical areas and 20 from randomly-selected normal areas. Based on analysis of the processed image histograms, it appeared that the density of vessel networks in the superficial layer of normal cortex (Fig. 6A, histogram in red) was greater than for epileptogenic cortex (Fig. 6A, histogram in blue). To facilitate statistical comparisons, each histogram was normalized to its area under the curve. As shown in Fig. 6B, a significant difference ($p < 0.05$) was detected mostly within the low-intensity range (6–26) between the normalized histograms obtained from epileptogenic and normal cortical areas, using a non-parametric permutation test. This suggests that the visually-perceivable blood vessels in epileptogenic cortical areas might be less than those found in normal areas within the superficial layer. However, the imaging penetration depths within the epileptogenic and normal cortical areas were unknown, and could be significantly different. Therefore, it is impossible to reach any quantitative conclusions regarding the vessel network densities in epileptogenic and normal cortical areas based upon current results. Nevertheless, some suspicion of altered vessel networks in epileptogenic cortex is justified.

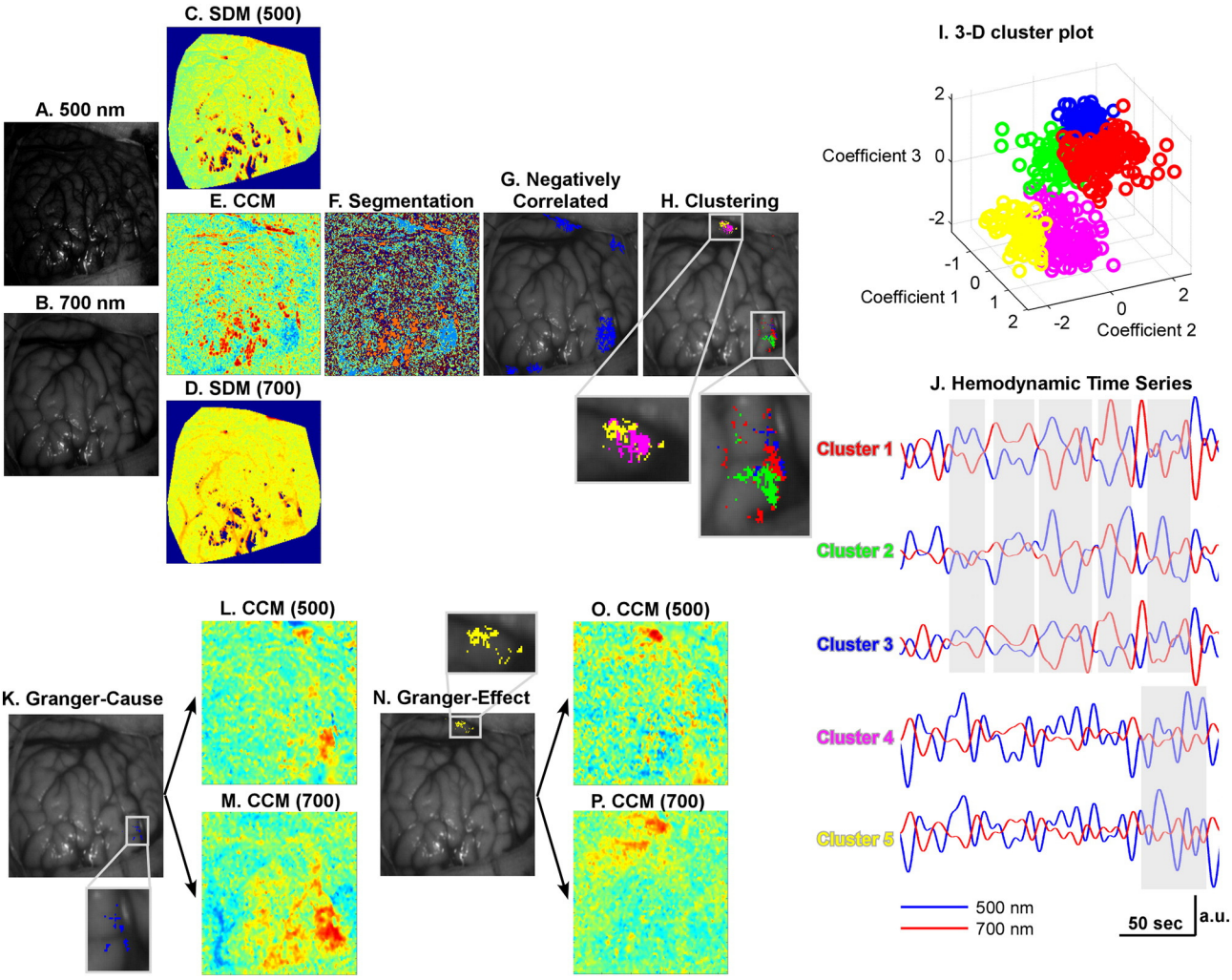

Fig. 3. Analysis of dynamic intrinsic optical signal imaging (DIOSI) data (Patient 1 as an example). (A) and (B) are the raw images obtained by DIOSI at 500 nm and 700 nm, respectively. Spectral density maps (SDMs) at 500 nm (C) and 700 nm (D) show the power of hemodynamic low-frequency oscillations (LFOs). The correlation coefficient map (CCM) in (E) was obtained by calculating the correlation coefficients between LFOs at the two wavelengths. K-means segmentation (F) was performed to isolate those regions with negative correlations (G). These regions were later classified into multiple clusters (H) by mean shift clustering. A 3-D color-coded scatter plot of the clustering features is shown in (I). Each cluster consists of LFOs with unique temporal profiles highlighted in gray boxes (J). A Granger causality toolbox was used to identify the Granger-cause (K) and Granger-effect (N) in each of these clusters. Seed-based CCM at both wavelengths were generated with regards to the Granger-cause (L for 500 nm, M for 700 nm) and Granger-effect (O for 500 nm, P for 700 nm). (For interpretation of the references to color in this figure legend, the reader is referred to the web version of this article.)

3.3. Functional features of the vascular network malformation

Intrinsic optical signals at 500 nm represent variations in CBV, while signals at 700 nm primarily reflect changes in oxygenation. In this study, the coupling mechanism between the change in CBV and that in oxygenation was investigated using an ARX model, wherein variations in oxygenation were considered output signals and those for CBV were treated as inputs. The IRFs obtained from the ARX model were capable of directly demonstrating the coupling mechanism between CBV and oxygenation. IRFs from the epileptogenic cortex and eloquent cortex appeared to be different in their temporal profiles. But there was no statistically-significant difference between the amplitudes of IRFs obtained from the epileptogenic and eloquent cortical areas (Fig. 7B). The training and testing data sets for the SVM classifier were extracted from the same recordings of each patient, but at different times. The SVM was applied to the training data sets to identify a hyper-plane that could identify differences between the IRFs obtained from epileptogenic ($n = 15$) versus eloquent areas ($n = 10$). Subsequently, the accuracy of differentiation was evaluated by applying the same SVM model to the testing data set. The accuracies of SVM models with ARX of different orders (5–40) were compared and are now illustrated in Fig. 7A. The ARX model at order 11 yielded the highest accuracy (84%) and the largest area under the ROC curve (0.82 out of 1) in SVM. We observed an optimal hyper-plane in SVM that was able to separate the IRFs of the epileptogenic cortical areas from those of the eloquent areas with a sensitivity of 93% and specificity of 70% (Fig. 7C).

4. Discussion

In the present study, the hemodynamic LFOs observed from the DIOSI recordings were an important biomarker differentiating epileptogenic cortex from normal eloquent areas. In addition, a significant difference between the vessel networks in epileptogenic cortex and normal brain area was identified. The proposed differentiation methodology involving LFOs relies neither on seizure attacks to localize epileptogenic cortex, nor on any external stimulation to map eloquent areas. Instead, it emphasizes the effective connectivity between various cortical regions, vessel network structures, and biophysical connections between changes in local blood volume and oxygenation. The feasibility of using this methodology for intraoperative guidance was tentatively evaluated using an SVM classifier to discriminate between epileptogenic and eloquent cortex.

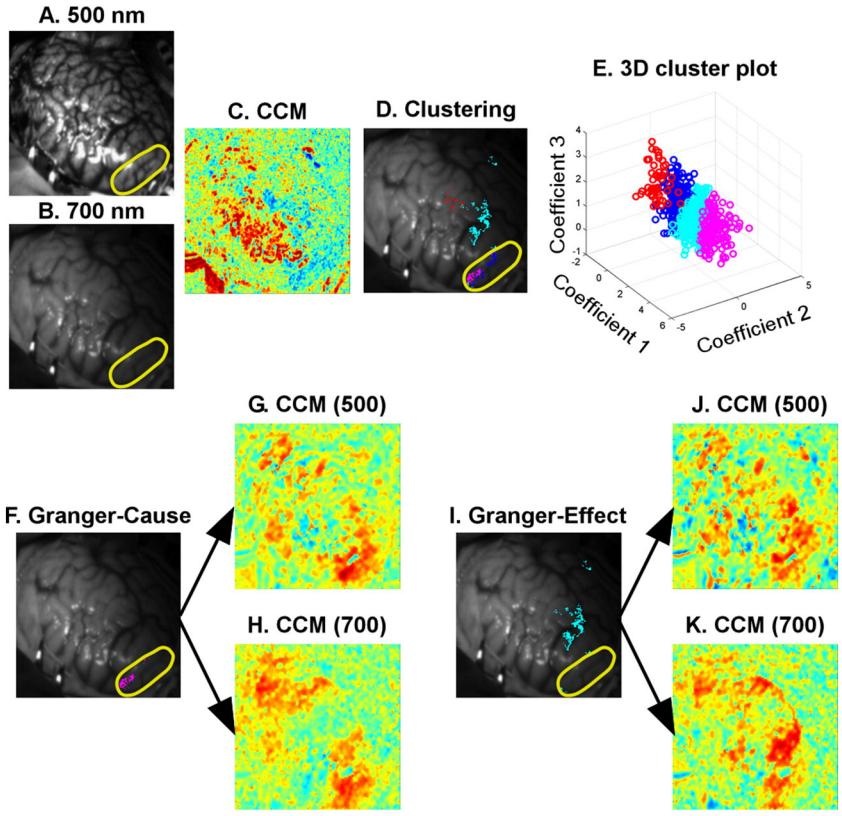

Fig. 4. Analysis of dynamic intrinsic optical signal imaging (DIOSI) data (Patient 2 as an example). (A) and (B) are the raw images obtained by DIOSI at 500 nm and 700 nm, respectively. The correlation coefficient map (CCM) in (C) was obtained by calculating the correlation coefficients between hemodynamic low-frequency oscillations (LFOs) at the two wavelengths. The negatively correlated regions were later classified into multiple clusters (D) by mean shift clustering. A 3-D scatter plot of the clustering features is shown in (E). A Granger causality toolbox was used to identify the Granger-cause (F) and Granger-effect (I) in each of these clusters. Seed-based CCM at both wavelengths were generated with regards to the Granger-cause (G for 500 nm, H for 700 nm) and Granger-effect (J for 500 nm, K for 700 nm). The resection area was outlined in yellow. (For interpretation of the references to color in this figure legend, the reader is referred to the web version of this article.)

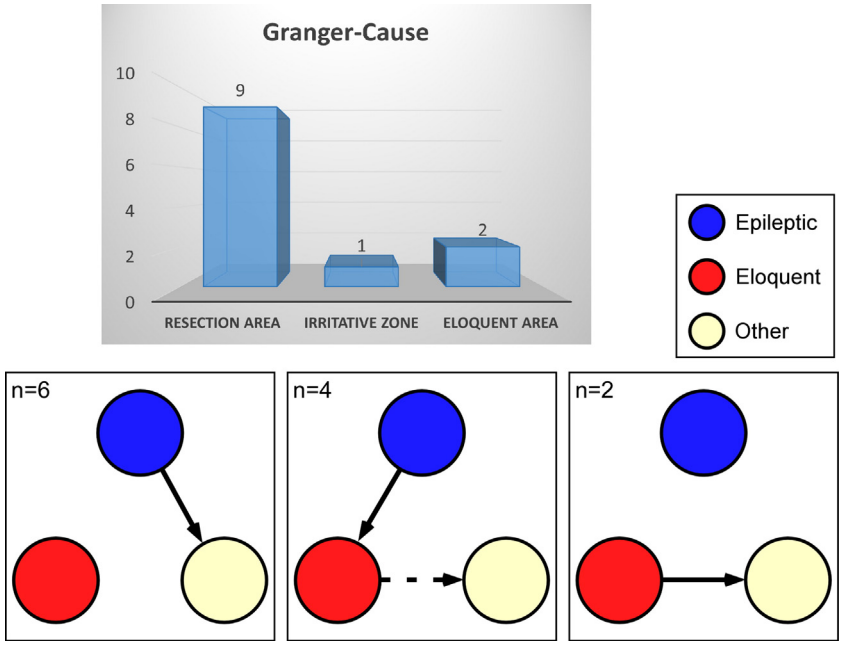

Fig. 5. Of the nine patients with resection areas inside the optical field of view (12 imaging data sets), 83% (n = 10, 9 in the resection area and 1 in an irritative zone) exhibited Granger-causes within epileptic cortex. Eloquent areas either directly contributed to the activities in a distant cortex (n = 2) or relayed activities from the epileptic (either resection area responsible for seizure onset or irritative zone) to some distant cortex (n = 4).

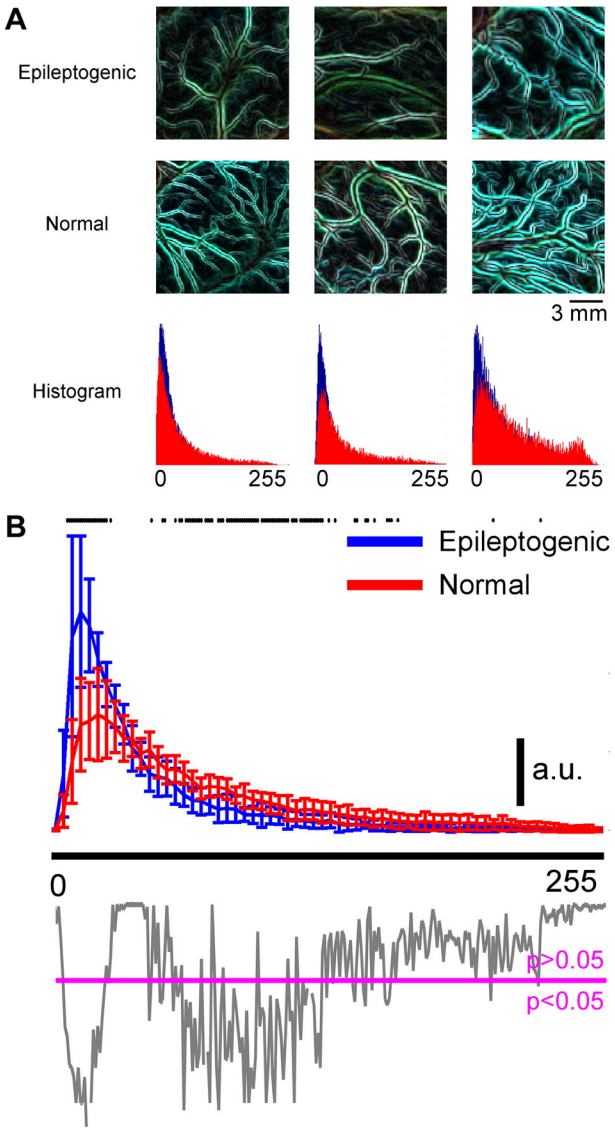

Fig. 6. Vasculature abnormalities in the superficial layer (anatomical features). A) Examples of vessel networks in epileptogenic and normal cortices and their corresponding histograms (blue: epileptogenic cortex, red: normal cortex). Areas showing normal cortex were randomly selected, regardless of their functional roles. B) Normalized histogram of the vessel network image obtained from the epileptogenic and normal cortices. Six patients (Patients 1, 2, 5, 7, 8, and 9) with high-quality color images of the exposed brain (number of epileptogenic areas = 18; number of normal areas = 20). For each patient, the window sizes for the epileptogenic and normal areas were the same. The histograms for each patient were normalized to the highest value in the epileptogenic area's histograms. The p-value from the permutation test (gray) was below the histogram with a magenta line showing the p-value equal to 0.05. Any p-value below the magenta line means there is a significant difference in the histograms at that intensity level. All statistically-significant intensity levels were highlighted in black dots at the top of the histograms. (For interpretation of the references to color in this figure legend, the reader is referred to the web version of this article.)

4.1. Hemodynamic low-frequency oscillations (LFOs)

The physiological signals centered in the in vivo study reported here are low-frequency, spontaneous, hemodynamic oscillations (<<0.1 Hz). This is an intrinsic property of the live brain, because these oscillations do not appear in brains after death (Nasiriavanaki et al., 2014). Hemodynamic LFOs have been attributed to resting-state functional activities (Mayhew et al., 1996, Toronov et al., 2000, Sliwka et al., 2001, Fox and Raichle, 2007; White et al., 2012, Song et al., 2012 and Nasiriavanaki et al., 2014). Rayshubskiy et al. (2014) found that slow sinusoidal hemodynamic oscillations were spatially localized to distinct regions of the cortex with tumors, exhibited wave-like propagation, and involved oscillations in the diameter of specific pial arterioles, indicating that the effect was not the result of systemic blood pressure oscillations. In the present study, LFOs tended to be local and their localizations were very reproducible from different observations, appearing in eloquent as well as epileptogenic cortical areas. This observation is in agreement with the suggestion by Fox and Raichle (2007) that, in addition to normal resting-state functional activities, LFOs may also be a manifestation of disease-related neural processing.

We employed sophisticated data analysis schemes to differentiate between the LFOs originating in eloquent cortex and those from epileptogenic cortex. The proposed methodology was used to identify differences in resting-state hemodynamic LFOs between the eloquent and epileptogenic cortical areas, in terms of brain connectivity and underlying biophysical mechanisms. Instead of relying solely on the magnitudes of LFOs (Song et al., 2012), the negative correlation between the DIOSI data at 500 nm and 700 nm was taken as an indication of underlying neuronal activity, which could be explained by the generally-accepted Balloon model (Buxton et al., 2004 and Buxton, 2012). However, the epileptogenic cortex in two studied patients exhibited a positive correlation between the intrinsic optical signals at the two wavelengths, suggesting that a different neurovascular coupling mechanism might exist. Little effort was devoted to the investigation of the cortical areas with positively-correlated LFOs in the current study, due to the limited number of cases, as well as their similarity to the artifacts caused by specular reflectance. For each case studied, epileptogenic cortex predominantly had directed influences on no less than one area, sometimes in close proximity and sometimes remote, probably because of different propagation mechanisms for the epileptiform discharges. This phenomenon was discussed previously by Song et al. when they studied a preclinical model of focal epilepsy (Song et al., 2015). Such connections were further investigated using the G-cause as the reference in seed-based spatial correlation analysis, which provides insights into the network in a global view and the different underlying phenomena in the DIOSI data. However, even though 83% of the G-causes were responsible for epileptiform discharges, investigating the effective connectivity between these identified regions alone lacks support from physiological-based theories and, hence, is not a good choice for demarcating resection zones during epilepsy surgery. In addition, studying brain connectivity using DIOSI is only applicable when the epileptogenic area is located within the FOV of the DIOSI which, in practice, is not always the case. Therefore, a better way to understand of the underlying biophysical mechanism between the observed optical data at 500 nm and 700 nm was devised to address the above-mentioned limitations.

4.2. Stochastic modeling to characterize underlying pathophysiology

The ARX modeling employed in the proposed methodology was adopted to identify those unique temporal variations in hemodynamics that occur in epileptogenic cortex during non-ictal periods. SVM based upon the outcome of the ARX modeling was very accurate at differentiating epileptogenic cortex from eloquent cortical areas. This success may be attributed to alterations in the vasculature network, as well as to neurovascular/neurometabolic couplings within the epileptogenic cortex. DIOSI at 500 nm is predominantly used to measure changes in CBV, modulated by activity-evoked dilation of the pial arterioles (Lavine et al., 2011). On the other hand, DIOSI at 700 nm is sensitive to variations in the oxygen content of blood within the venous network (Lavine et al., 2011). Through ARX modeling of both DIOSI signals, the dynamic interplay between the arteriolar and venous networks (i.e., vasculature characteristics) was examined. The same approach should also reveal regional neuro-activity and neuro-metabolism, because of the neurovascular and neurometabolic coupling mechanisms that exist within the capillary bed that forms the bridge between the arteriolar and venous networks. From a neurovascular coupling point of

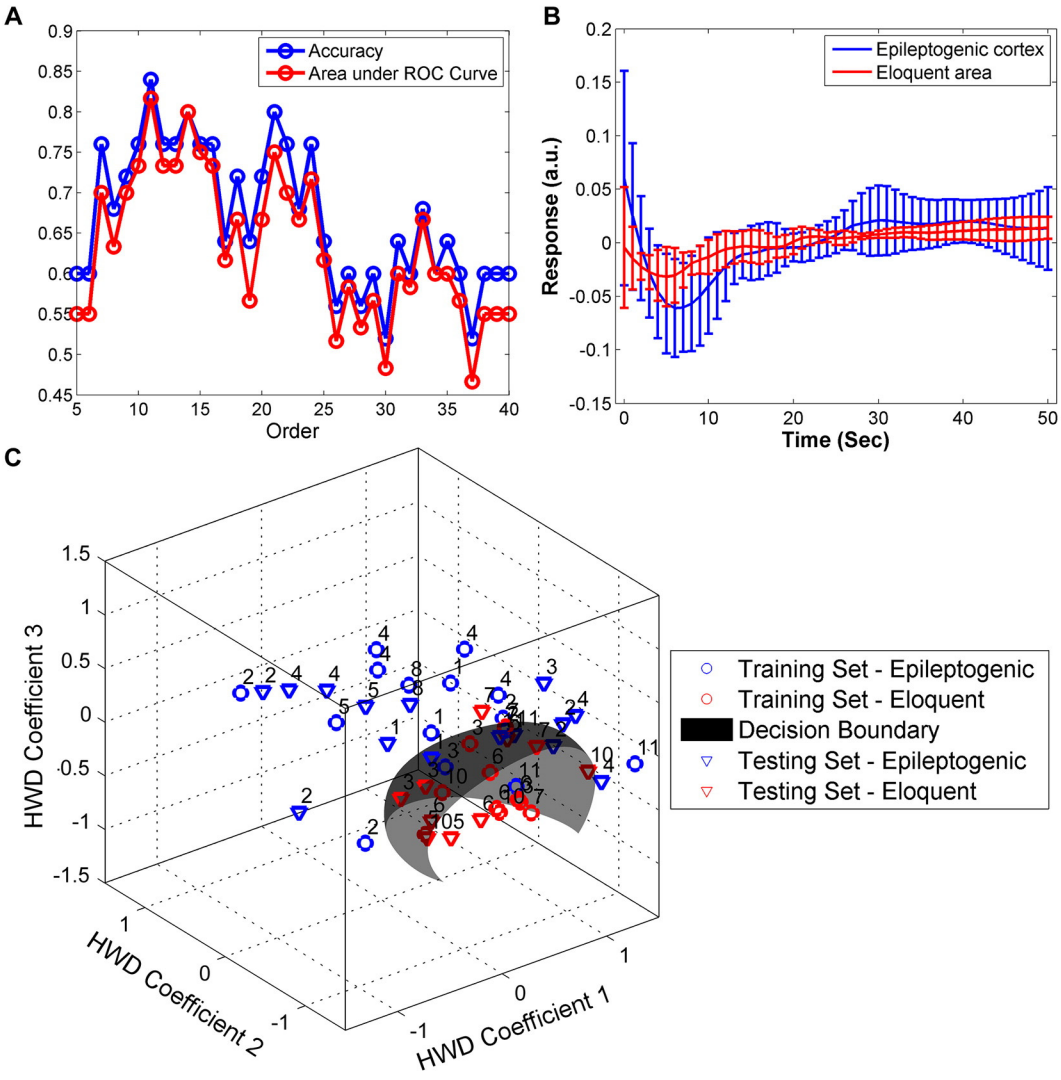

Fig. 7. Differentiation between epileptogenic and eloquent cortex based on functional features of vascular networks of all patients. (A) Autoregressive model with an exogenous source (ARX) at Order 11 shows the greatest accuracy (0.84) and largest area under the receiver operating characteristic (ROC) curve (0.82). (B) The corresponding impulse response functions (IRFs) obtained from epileptogenic (blue) and eloquent (red) areas. (C) The hyper-plane obtained by support vector machine (SVM) was able to separate epileptogenic cortex from eloquent areas with a sensitivity of 93% and a specificity of 70% (n = 25, 15 epileptogenic and 10 eloquent areas). The patient ID number is showing on top of each scatter point. HWD = Haar wavelet decomposition. (For interpretation of the references to color in this figure legend, the reader is referred to the web version of this article.)

view, astrocytes (McCaslin et al., 2011), pericytes (Hamilton et al., 2010) and endothelium (Chen et al., 2014) play critical roles in the coupling mechanism. Both pericyte degeneration and thickening of microvessel walls have been found in the abnormally-spiking brain areas detected in patients with intractable complex partial epilepsy (Liwnicz et al., 1990). In addition, vascular malformations have been frequently identified in association with focal epilepsy (Ndode-Ekane et al., 2010, Spreafico and Blümcke, 2010 and Cui and Luan, 2011). Moreover, relative to low-spiking areas, increased vascularity and microglial infiltration have been demonstrated in high-spiking human neocortex (Dachet et al., 2014). As for alterations in neurometabolic coupling, regional hypometabolism, both in cortical and subcortical areas, has been demonstrated in preclinical seizure models (Jupp et al., 2012 and Choi et al., 2014). Finally, the outcomes of anatomical vasculature analysis identified in this study also reveal significant differences in vasculature density within the visually-perceivable superficial layer between epileptogenic and normal cortical areas. This being said, the imaging technique used in this study lacked the resolution, contrast, and penetration depth for us to further investigate the exact source of the abnormalities.

4.3. Implications for pre-operative fMRI techniques

As discussed above, the relationship between the LFOs obtained by DIOSI at 500 nm and 700 nm could be used as a biomarker to distinguish epileptogenic from normal/eloquent cortex. Because of its limited penetration depth, it is not feasible to use DIOSI to detect deep-seated epileptogenic foci. In addition, the success of DIOSI at mapping epileptogenic cortex intraoperatively depends highly on accurate pre-operative localizations based on other neuro-imaging modalities. That being said, if the pre-operative imaging fails to provide sufficient information to localize all the epileptogenic cortices, the DIOSI will be limited to detecting only those that are located inside the exposed cortical areas. Unfortunately, despite all the current technologies available for epilepsy surgery, only about 62.4% of epilepsy surgery patients achieve a good post-operative outcome (Jobst and Cascino, 2015). Patients 1 and 5 in this study exhibited recurrent seizures after surgery, which indicates current deficiencies in our understanding of epileptogenesis in focal epilepsy. Consequently, non-invasively detecting all epileptogenic areas pre-operatively is essential if intraoperative DIOSI is to delineate them. Unfortunately, such pre-operative detection remains a challenge.

Since fluctuations in DIOSI at 500 nm and 700 nm are related to changes in CBV and oxygenation, it is possible to detect these physiological characteristics using non-invasive imaging modalities like fMRI. Functional MRI is capable of measuring blood oxygenation level dependent (BOLD) signals that are associated with regional hemodynamics, as well as metabolic parameters like the oxygen extraction ratio, $CMRO_2$, CBF and CBV. In addition, fMRI can measure vascular space occupancy (VASO), which provides indirect access to the changes in CBV associated with neuronal activity (Lu et al., 2003). Recently, simultaneous BOLD-fMRI and VASO-fMRI have been performed to study functionally-induced BOLD and CBV responses in human brain (Yang et al., 2004 and Krieger et al., 2014). Consequently, the same technique can be used to acquire BOLD and CBV signals from epileptogenic brain in a non-invasive fashion, with data interpreted using the approaches disclosed in the current study, thereby allowing for epileptogenic cortex to be identified and separated from normal/eloquent cortex. This combination would be remarkably crucial to the precise detection of deep epileptogenic brain areas during the pre-operative planning phase.

4.4. Consideration of anesthesia

In this study, all patients were anesthetized using a combination of propofol and fentanyl (Table 2). Propofol is one of the most popular anesthetic agents used in epilepsy surgery. It is also highly recommended for use in fMRI studies, since it has relatively minor effects on hemodynamic responses (Ding and White, 2002) and does not inhibit stimulus-evoked cortical activity in either animals or humans (Kalkman et al., 1991 and Scanley et al., 1997). Unfortunately, according to a study by Zijlmans et al. (2012), the infusion of propofol alone could have an antiepileptic effect and lead to reductions in certain epileptic activity. Dose-dependent propofol alone could also change cortical and subcortical functional connectivity during the resting state (Boveroux et al., 2010, Mhuircheartaigh et al., 2010 and Stamatakis et al., 2010). Recently, Rayshubskiy et al. (2014) reported the results of their DIOSI and fMRI study on two patients. The investigators were able to observe ~0.1 Hz hemodynamic oscillations within the cortex of the one patient kept awake while undergoing brain tumor surgery, but not in the patient who had been anesthetized with propofol during epilepsy surgery (note that this epileptic patient was a 36-year-old male, and that the underlying pathology was not disclosed). The use of propofol alone might be the reason that the investigators were unable to detect hemodynamic LFOs in the epileptogenic cortex. It has also been reported that propofol has a potential pro-convulsant effect. Cheng et al. (1996) have suggested that the reported pro-convulsant effects of propofol could be a result of combining propofol with other anesthetic agents like ketamine and fentanyl. This hypothesis is supported by the results of other studies (Hufnagel et al., 1990, Wang et al., 2012 and Yalcin et al., 2012). Based on this evidence, those hemodynamic LFOs observed in eloquent and epileptogenic cortical areas should definitely have their origins in resting-state neuronal activity and epileptic activity, respectively.

4.5. Significance and limitations

The methods proposed here to identify epileptogenic cortex could be conducted on epilepsy patients under anesthesia during surgery. They do not require any external stimulation or any reduction in anesthesia to map eloquent areas. This makes DIOSI a promising, complementary tool for intraoperative guidance. It could also provide more specific direction regarding where to place subdural electrodes for ECoG recordings.

However, due to the limited penetration depth of visible light into biological tissues, DIOSI can only investigate pathophysiological characteristics within the superficial layer of the cortex, a limitation that is similar to that of ECoG using surface electrode arrays (Gasser et al., 2005). In addition, DIOSI is susceptible to artifacts induced by specular reflection, because human cortical surfaces are not flat. To overcome these artifacts of specular reflection, DIOSI acquisition could be focused on one area of the exposed cortical surface at a time, as well as at different locations and from different viewing angles.

Another limitation to consider is that our study was conducted on pediatric patients with focal epilepsy, usually accompanied by lesions in the cortex. The feasibility of using the same methods for other types of epilepsy or on different populations remains to be investigated.

5. Conclusions

For this study, a new methodology of intraoperative optical imaging was proposed to detect and differentiate epileptogenic from eloquent cortex in pediatric patients with focal epilepsy. The proposed methodology was based on the effective connectivity, underlying biophysical mechanisms, and vasculature network characteristics of the cortical surface. Together, this creates a new means of intraoperative epileptogenic cortex localization that is both economical and effective at the same time. More importantly, this analysis based on biophysical mechanisms can differentiate between eloquent and epileptogenic cortex with high sensitivity and specificity. Neither external stimulation nor reduced anesthesia is required, both of which are required for current intraoperative monitoring techniques. More importantly, the analytical methods revealed in this manuscript can be applied to data obtained from simultaneous BOLD- and VASO-fMRI, as well as from other non-invasive optical imaging modalities capable of acquiring hemodynamic LFOs from the brain. The incorporation of this new methodology could positively impact the outcomes of epilepsy surgery in pediatric patients.

Funding

This work was supported by Nicklaus Children's Hospital and the Ware Foundation.

Acknowledgements

The authors would like to express gratitude to the nurses and staffs at Nicklaus Children's Hospital who helped to conduct the in vivo studies.

References

Alarcon, G., et al., 1997. Origin and propagation of interictal discharges in the acute electrocorticogram. Brain 120, 2259–2282.
Boveroux, P., et al., 2010. Breakdown of within-and between-network resting state functional magnetic resonance imaging connectivity during propofol-induced loss of consciousness. Anesthesiology 113 (5), 1038–1053.
Buxton, R.B., 2012. Dynamic models of BOLD contrast. NeuroImage 62 (2), 953–961.
Buxton, R.B., Uludağ, K., Dubowitz, D.J., Liu, T.T., 2004. Modeling the hemodynamic response to brain activation. NeuroImage 23, S220–S233.
Cannestra, A.F., et al., 2000. Temporal and topographical characterization of language cortices using intraoperative optical intrinsic signals. NeuroImage 12 (1), 41–54.
Cannestra, A.F., et al., 2001. Temporal spatial differences observed by functional MRI and human intraoperative optical imaging. Cereb. Cortex 11 (8), 773–782.
Chaplot, S., Patnaik, L., Jagannathan, N., 2006. Classification of magnetic resonance brain images using wavelets as input to support vector machine and neural network. Biomed. Signal Process. Control 1 (1), 86–92.
Chen, B.R., Kozberg, M.G., Bouchard, M.B., Shaik, M.A., Hillman, E.M., 2014. A critical role for the vascular endothelium in functional neurovascular coupling in the brain. J. Am. Heart Assoc. 3 (3), e000787.
Cheng, M.A., et al., 1996. Large-dose propofol alone in adult epileptic patients: electrocorticographic results. Anesth. Analg. 83 (1), 169–174.
Choi, H., et al., 2014. Abnormal metabolic connectivity in the pilocarpine-induced epilepsy rat model: a multiscale network analysis based on persistent homology. NeuroImage 99, 226–236.
Cui, Z., Luan, G., 2011. A venous malformation accompanying focal cortical dysplasia resulting in a reorganization of language-eloquent areas. J. Clin. Neurosci. 18 (3), 404–406.
Dachet, F., et al., 2014. Predicting novel histopathological microlesions in human epileptic brain through transcriptional clustering. Brain (awu350).
Ding, Z., White, P.F., 2002. Anesthesia for electroconvulsive therapy. Anesth. Analg. 94 (5), 1351–1364.

El-Naqa, I., Yang, Y., Wernick, M.N., Galatsanos, N.P., Nishikawa, R.M., 2002. A support vector machine approach for detection of microcalcifications. IEEE Trans. Med. Imaging 21 (12), 1552–1563.
Fox, M.D., Raichle, M.E., 2007. Spontaneous fluctuations in brain activity observed with functional magnetic resonance imaging. Nat. Rev. Neurosci. 8 (9), 700–711.
Gasser, T., et al., 2005. Intraoperative functional MRI: implementation and preliminary experience. NeuroImage 26 (3), 685–693.
Glover, G.H., 1999. Deconvolution of impulse response in event-related BOLD fMRI 1. NeuroImage 9 (4), 416–429.
Guo, L., Rivero, D., Dorado, J., Rabunal, J.R., Pazos, A., 2010. Automatic epileptic seizure detection in EEGs based on line length feature and artificial neural networks. J. Neurosci. Methods 191 (1), 101–109.
Haglund, M.M., Hochman, D.W., 2004. Optical imaging of epileptiform activity in human neocortex. Epilepsia 45 (s4), 43–47.
Hamilton, N.B., Attwell, D., Hall, C.N., 2010. Pericyte-mediated regulation of capillary diameter: a component of neurovascular coupling in health and disease. Front. Neuroenerg. 2.
Hufnagel, A., Elger, C., Nadstawek, J., Stoeckel, H., Böker, D., 1990. Specific response of the epileptic focus to anesthesia with propofol. J. Epilepsy 3 (1), 37–45.
Jayakar, P., Duchowny, M., Resnick, T.J., 1994. Subdural monitoring in the evaluation of children for epilepsy surgery. J. Child Neurol. 9 (2 suppl.), 2S61–62S66.
Jayakar, P., et al., 2008. Epilepsy surgery in patients with normal or nonfocal MRI scans: integrative strategies offer long-term seizure relief. Epilepsia 49 (5), 758–764.
Jobst, B.C., Cascino, G.D., 2015. Resective epilepsy surgery for drug-resistant focal epilepsy: a review. JAMA. 313 (3), 285–293.
Jupp, B., et al., 2012. Hypometabolism precedes limbic atrophy and spontaneous recurrent seizures in a rat model of TLE. Epilepsia 53 (7), 1233–1244.
Kalkman, C., Traast, H., Zuurmond, W., Bovill, J., 1991. Differential effects of propofol and nitrous oxide on posterior tibial nerve somatosensory cortical evoked potentials during alfentanil anaesthesia. Br. J. Anaesth. 66 (4), 483–489.
Krieger, S.N., Huber, L., Poser, B.A., Turner, R., Egan, G.F., 2014. Simultaneous acquisition of cerebral blood volume-, blood flow-, and blood oxygenation-weighted MRI signals at ultra-high magnetic field. Magn. Reson. Med.
Krsek, P., et al., 2013. Predictors of seizure©\free outcome after epilepsy surgery for pediatric tuberous sclerosis complex. Epilepsia 54 (11), 1913–1921.
Lavine, M., Haglund, M.M., Hochman, D.W., 2011. Dynamic linear model analysis of optical imaging data acquired from the human neocortex. J. Neurosci. Methods 199 (2), 346–362.
Liwnicz, B.H., Leach, J.L., Yeh, H.-S., Privitera, M., 1990. Pericyte degeneration and thickening of basement membranes of cerebral microvessels in complex partial seizures: electron microscopic study of surgically removed tissue. Neurosurgery 26 (3), 409–420.
Lu, H., Golay, X., Pekar, J.J., van Zijl, P., 2003. Functional magnetic resonance imaging based on changes in vascular space occupancy. Magn. Reson. Med. 50 (2), 263–274.
Luo, Q., et al., 2013. Spatio-temporal Granger causality: a new framework. NeuroImage 79, 241–263.
Mallat, S.G., 1989. A theory for multiresolution signal decomposition: the wavelet representation. IEEE Trans. Pattern Anal. Machine Intell. 11 (7), 674–693.
Mayhew, J.E., et al., 1996. Cerebral vasomotion: a 0.1-Hz oscillation in reflected light imaging of neural activity. NeuroImage 4 (3), 183–193.
McCaslin, A.F., Chen, B.R., Radosevich, A.J., Cauli, B., Hillman, E.M., 2011. In vivo 3D morphology of astrocyte–vasculature interactions in the somatosensory cortex: implications for neurovascular coupling. J. Cereb. Blood Flow Metab. 31 (3), 795–806.
Mhuircheartaigh, R.N., et al., 2010. Cortical and subcortical connectivity changes during decreasing levels of consciousness in humans: a functional magnetic resonance imaging study using propofol. J. Neurosci. 30 (27), 9095–9102.
Nasiriavanaki, M., et al., 2014. High-resolution photoacoustic tomography of resting-state functional connectivity in the mouse brain. Proc. Natl. Acad. Sci. 111 (1), 21–26.
Ndode-Ekane, X., Hayward, N., Gröhn, O., Pitkänen, A., 2010. Vascular changes in epilepsy: functional consequences and association with network plasticity in pilocarpine-induced experimental epilepsy. Neuroscience 166 (1), 312–332.
Paolicchi, J., et al., 2000. Predictors of outcome in pediatric epilepsy surgery. Neurology 54 (3), 642-642.
Pondal-Sordo, M., Diosy, D., Téllez-Zenteno, J.F., Sahjpaul, R., Wiebe, S., 2007. Usefulness of intracranial EEG in the decision process for epilepsy surgery. Epilepsy Res. 74 (2), 176–182.
Ramírez, J., et al., 2013. Computer-aided diagnosis of Alzheimer's type dementia combining support vector machines and discriminant set of features. Inf. Sci. 237, 59–72.
Rayshubskiy, A., et al., 2014. Direct, intraoperative observation of ~0.1 Hz hemodynamic oscillations in awake human cortex: implications for fMRI. NeuroImage 87, 323–331.
Rigau, V., et al., 2007. Angiogenesis is associated with blood–brain barrier permeability in temporal lobe epilepsy. Brain 130 (7), 1942–1956.
Roebroeck, A., Formisano, E., Goebel, R., 2005. Mapping directed influence over the brain using Granger causality and fMRI. NeuroImage 25 (1), 230–242.
Sato, K., et al., 2002. Intraoperative intrinsic optical imaging of neuronal activity from subdivisions of the human primary somatosensory cortex. Cereb. Cortex 12 (3), 269–280.
Scanley, B.E., et al., 1997. Functional magnetic resonance imaging of median nerve stimulation in rats at 2.0 T. Magn. Reson. Med. 37 (6), 969–972.
Sliwka, U., et al., 2001. Spontaneous oscillations in cerebral blood flow velocity give evidence of different autonomic dysfunctions in various types of headache. Headache 41 (2), 157–163.
Sobottka, S.B., et al., 2013. Intraoperative optical imaging of intrinsic signals: a reliable method for visualizing stimulated functional brain areas during surgery: clinical article. J. Neurosurg. 119 (4), 853–863.
Sommer, B., et al., 2013. Integration of functional neuronavigation and intraoperative MRI in surgery for drug-resistant extratemporal epilepsy close to eloquent brain areas. Neurosurg. Focus. 34 (4), E4.
Song, Y., et al., 2012. Low-frequency pathophysiological characteristics of pediatric epileptic cortex during the interictal period detected using a dual-wavelength imaging system. SPIE Medical Imaging, (International Society for Optics and Photonics) (83170 V-83170 V-83178).
Song, Y., Sanganahalli, B.G., Hyder, F., Lin, W.-C., Riera, J.J., 2015. Distributions of irritative zones are related to individual alterations of resting-state networks in focal epilepsy. PLoS ONE 10 (7), e0134352.
Spreafico, R., Blümcke, I., 2010. Focal cortical dysplasias: clinical implication of neuropathological classification systems. Acta Neuropathol. 120 (3), 359–367.
Stamatakis, E.A., Adapa, R.M., Absalom, A.R., Menon, D.K., 2010. Changes in resting neural connectivity during propofol sedation. PLoS ONE 5 (12), e14224.
Subasi, A., Gursoy, M.I., 2010. EEG signal classification using PCA, ICA, LDA and support vector machines. Expert Syst. Appl. 37 (12), 8659–8666.
Suh, M., Bahar, S., Mehta, A.D., Schwartz, T.H., 2006. Blood volume and hemoglobin oxygenation response following electrical stimulation of human cortex. NeuroImage 31 (1), 66–75.
Tharin, S., Golby, A., 2007. Functional brain mapping and its applications to neurosurgery. Neurosurgery 60 (4), 185–202.
Toronov, V., et al., 2000. Near-infrared study of fluctuations in cerebral hemodynamics during rest and motor stimulation: temporal analysis and spatial mapping. Med. Phys. 27 (4), 801–815.
Wang, X., et al., 2012. Effects of propofol and ketamine as combined anesthesia for electroconvulsive therapy in patients with depressive disorder. J. ECT 28 (2), 128–132.
White, B.R., Liao, S.M., Ferradal, S.L., Inder, T.E., Culver, J.P., 2012. Bedside optical imaging of occipital resting-state functional connectivity in neonates. NeuroImage 59 (3), 2529–2538.
Winston, G.P., 2013. Epilepsy surgery, vision, and driving: what has surgery taught us and could modern imaging reduce the risk of visual deficits? Epilepsia 54 (11), 1877–1888.
Yalcin, S., et al., 2012. Ketofol in electroconvulsive therapy anesthesia: two stones for one bird. J. Anesth. 26 (4), 562–567.
Yang, Y., Gu, H., Stein, E.A., 2004. Simultaneous MRI acquisition of blood volume, blood flow, and blood oxygenation information during brain activation. Magn. Reson. Med. 52 (6), 1407–1417.
Zavar, M., Rahati, S., Akbarzadeh-T, M.-R., Ghasemifard, H., 2011. Evolutionary model selection in a wavelet-based support vector machine for automated seizure detection. Expert Syst. Appl. 38 (9), 10751–10758.
Zijlmans, M., et al., 2012. Epileptic high-frequency oscillations in intraoperative electrocorticography: the effect of propofol. Epilepsia 53 (10), 1799–1809.